CCFE
CULHAM CENTRE FOR FUSION ENERGY

UK Atomic Energy Authority

UKAEA-CCFE-PR(18)31

S. S. Henderson, M. M. Bluteau, M. G. O'Mullane and H. P. Summers

Improvements of impurity line power coefficients relevant to ITER and DEMO via systematic optimisation of atomic structure

Improvements of impurity line power coefficients relevant to ITER and DEMO via systematic optimisation of atomic structure

S. S. Henderson,[1, 2] M. M. Bluteau,[1] M. G. O'Mullane[1] and H. P. Summers[1]

[1]*Department of Physics SUPA, University of Strathclyde, Glasgow, G4 0NG, UK*
[2]*CCFE, Culham Science Centre, OX14 3DB, UK*

This is a preprint of a paper submitted for publication in
Plasma Physics and Controlled Fusion

Improvements of impurity line power coefficients relevant to ITER and DEMO via systematic optimisation of atomic structure

S. S. Henderson[1,2], M. M. Bluteau[1], M. G. O'Mullane[1], H. P. Summers[1]

[1] Department of Physics SUPA, University of Strathclyde, Glasgow, G4 0NG, UK
[2] CCFE, Culham Science Centre, OX14 3DB, UK

E-mail: stuart.henderson@ukaea.uk

Abstract. Spectra line power by medium and heavy weight elements is a main source of radiative loss in tokamak plasma and sets operational limits on the design of ITER and DEMO. The preferred comprehensive basis of impurity line power coefficients provided by ADAS is theoretical, using the Autostructure code with distorted wave electron impact cross-sections replacing earlier use of the Cowan code with plane-wave Born cross-sections. Autostructure uses orbital scaling parameters in radial wavefunction generation, which, at default settings, yield uncertainies of up to 30% in the line power coefficients. A set of orbital scaling parameters is presented for every ion up to the Pd-like iso-electronic sequence using a systematic optimisation scheme. These optimised scaling parameters are used with semi-relativistic, distorted wave Autostructure calculations and reduce the uncertainty in the line power coefficients due to the atomic structure inaccuracy to $\leq 5\%$. The new line power coefficients differ from the previous Cowan baseline coefficients by up to 15%. Remaining uncertainty in the composite cooling function is attributed to the fractional ion abundance inaccuracy.

1. Introduction

Use of scaling parameters in the model central potential determining the radial wavefunctions (orbitals) is typical of atomic structure codes such as Autostructure. Optimisation of these parameters in association with observed energy levels or transition probabilities is a requirement for comparative spectroscopic analysis concerning ion emission, including detailed studies of specific line intensities or gross calculations of total radiated line power coefficients. For example, line ratios used to determine the volumetric plasma properties (e.g. [1–3]) rely on the accuracy of the theoretical radiative data to identify the wavelengths of lines within a spectrum and to compute the line brightness. For future tokamak designs, such as ITER and DEMO, the line power radiated by the medium/heavy impurity ions in the core plasma limits the operational parameter space and therefore system codes, such as *process* and *sycomore* [4–6], rely on the accuracy of these theoretical impurity line power coefficients [7].

Ideally, these coefficients are calculated using a collisional-radiative model with verified energy level and transition probability data and high quality collision data from close-coupled methods, such as R-matrix. The Atomic Database Analysis Structure (ADAS) [8] collects and provides these high quality data, if they exist, and supplements any missing data with baseline data computed using Cowan's code [9] and its plane-wave Born (PWB) cross-section calculation. The elements expected in modern and future tokamak plasmas vary widely, from wall materials including C, Be and W, and Mo, to injected gases including N, Ne, Ar, Kr, and Xe. Thus the supporting baseline calculations are relied on increasingly frequently, especially for element heavier that Ar, and their accuracy is an on-going concern.

A programe is underway to improve the baseline calculations in ADAS by using the Autostructure code [10,11] (AS) which includes internal determination of distorted wave (DW) electron impact collision strengths. PWB is a valid high energy approximation, but does not include spin change, whereas DW calculations include spin-changing transitions and improve the accuracy in the medium/threshold energy region. Neither PWB or DW calculations include resonances. The accuracy of the line power coefficients and collision strengths also rely on the quality of the atomic structure. The improvement programme has two parts, firstly ensuring inclusion of all configurations contributing significantly to the radiated power for an ion [12] and secondly, optimising the atomic structure through the orbital scaling parameters - the object of this paper. The radial wavefunctions are computed in AS using a Thomas-Fermi-Dirac-Amaldi (TFDA) model potential [13], in contrast to the Hartree-Fock method used by Cowan [9]. The TFDA method, without any optimisation of the radial wavefunctions, that is with orbital scaling factors set to unity, was shown to introduce further uncertainties in the line power coefficients which could outweigh any improvements gained from DW [12].

Numerous studies exist demonstrating different structure optimisation strategies for AS; however these are either limited to single ion studies (e.g. Ar III, Si II, O III, Co II, and Co III) [1,2,14–16] or single iso-electronic sequence studies (e.g. Be-, B-, F-, Ne-, and Mg-like) [17–21]. Currently, no thorough, systematic study exists that covers the optimisation of all the heavier weight species found in tokamak plasma, recognising both iso-nuclear and iso-electronic trends. Therefore, this paper demonstrates a systematic structure optimisation strategy for any ion and element to improve the accuracy of the atomic structure data computed by AS to at least the same standard produced by Cowan's code and where possible to near measured energy level standards.

The paper is structured as follows. Section 2 outlines the optimisation strategy and discusses the results of the optimisation iso-electronically and iso-nuclearly. The improvement in accuracy of the atomic structure data following the optimisation is quantified in section 3. Quantitative assessment measures are used based on the average oscillator strength, the energy level accuracy, and the radiated line power coefficients. The conclusions are presented in section 5.

2. Optimisation strategy

AS calculates semi-relativistic radial wavefunctions using the TFDA model potential $V_{TFDA}(\lambda_{nl})$ [13], where λ_{nl} are the radial scaling parameters applied to each nl orbital. The λ_{nl} values are optimised internally within AS to minimise the weighted sum of all LS term energies. For any ion, this minimisation can be carried out for all relevant orbitals as part of the calculation.

Minimising every λ_{nl} over every term included in the calculation can dilute the correlations between subsets of terms and λ_{nl}. In this scenario, the minimisation can lead to anomalous values of λ_{nl}; that is, values which do not improve (or cause a degredation of) the accuracy or that differ significantly from values obtained from nearby ions in an iso-electronic or iso-nuclear sequence. The dilution can be avoided either by reducing the number λ_{nl} included in the optimisation, or by only including the most strongly correlated terms in the minimisation. The trends of λ_{nl} as a function of iso-electronic and iso-nuclear sequence can further help to identify (and remove) any anomalous λ_{nl} values.

One strategy to reduce this dilution effect suggests fixing the inner shell λ_{nl} to pre-determined, optimised values whilst only allowing minimisation of the ground and valence orbitals [22]. This strategy is adopted in this paper. In each iso-electronic sequence, the configuration basis set is determined using a rule-based algorithm that provides the most significant configurations contributing to the power within a pre-defined set of (level) limits [12]. The rules were adjusted for this study to limit the electron promotions from the metastable configurations to $\Delta n \leq 2$ and to include the ground complex configurations. These configuration sets were sufficient to account for configuration interaction, whilst not significantly diluting the minimisation.

Strictly, the configuration sets contributing most significantly to the power are unique for each ion within an iso-electronic sequence; weakly charged ions with highly populated metastables may have a different set of optimised configurations to highly charged ions. Furthermore, inner shell promotions are significant as the ion charge increases. In this analysis, the same configuration basis set is used for all ions in a sequence using W as the optimising element. This simplification did not significantly change the iso-electronic scaling parameter trends shown later in figure 1. The configuration sets for each sequence are available as supplementary data in ADAS adf27 form‡, the ADAS data format for AS driver files.

‡ See ADAS manual http://adas.ac.uk/manual.php for formatting conventions.

Table 1. Orbital scaling parameter minimisation setup in the AS code

	Fixed	Free	Tied
Li−Mg-like	−	$\lambda_{1s}, \lambda_{2s}, \lambda_{2p}, \lambda_{3d}$	$\lambda_{3s}, \lambda_{3p}, \lambda_{4s}, \lambda_{4p}$
Al−Kr-like	$\lambda_{1s}, \lambda_{2s}, \lambda_{2p}$	$\lambda_{3s}, \lambda_{3p}, \lambda_{3d}, \lambda_{4f}$	$\lambda_{4s}, \lambda_{4p}, \lambda_{4d}$
Rb−Pd-like	$\lambda_{1s}, \lambda_{2s}, \lambda_{2p}, \lambda_{3s}, \lambda_{3p}, \lambda_{3d}$	$\lambda_{4s}, \lambda_{4p}, \lambda_{4d}, \lambda_{4f}$	$\lambda_{5s}, \lambda_{5p}, \lambda_{5d}, \lambda_{5f}$

To determine the optimised values of the inner core λ_{nl} of a particular ion, it is necessary to firstly assess the iso-electronic sequences with an open $1s$ shell, then those with an open $2s$ shell, and so on up to the ground orbital of the ion. The assumption in this systematic approach is that closed-shell λ_{nl} values do not vary from one iso-electronic sequence to another. Note that the λ_{nl} are still varied for at-least two sequences after becoming core orbitals to verify this assumption. In addition to fixing the inner core λ_{nl} in the minimisation, it is also possible to tie together scaling parameters of equal l and thus set $lambda_{nl} \equiv \lambda_l$; this matches the original description described in [13]. In this paper, nl-dependent λ_{nl} values are used for the fixed inner core orbitals, and then tied for equal l for the remaining ground and valence orbitals. An overview of the optimisation setup for all iso-electronic sequences is given in table 1.

Sequences from Li-like to Mg-like are first investigated. The results of the optimisation for the λ_{1s}, λ_{2s}, and λ_{2p} are shown in figure 1a-c. Within an iso-electronic sequence, a decay towards unity is found for both λ_{1s} and λ_{2s} with increasing Z_0. The opposite trend is observed for λ_{2p} which rises significantly at high Z_0. Currently, the cause of the latter trend is unclear; however it could be explained in terms of the sensitivity of the TFDA potential to λ_{nl}. As Z_0 increases, the Coulomb potential dominates and therefore bigger changes to λ_{nl} are required to have an effect. This assumption is discussed in the following section.

Lastly, and most significantly, as the iso-electronic sequence increases the λ_{nl} values begin to overlap as a function of Z_0. For the λ_{1s}, $\lambda_{2s}$and λ_{2p} values, this occurs at Na-like and Mg-like as shown by the red and green curves in figures 1a-c. These λ_{nl} values are therefore fixed for all consequent iso-electronic sequences.

Optimised λ_{nl} values for a selecton of the lower iso-sequences (Be, B, F, Ne, and Mg -like) have been previously documented [17–21]. Reasonable agreement between the previous literature and the study presented here is found at low nuclear charge; however deviations are found at higher nuclear charge. This deviation occurs because the previous studies focus on R-matrix collision calculations and therefore only include relativistic Breit-Pauli correction terms perturbatively; whereas this study uses kappa-averaged semi-relativistic wavefunctions. For heavy species, relativistic effects can no longer be treated as a perturbation.

The next set of iso-electronic sequences from Al-like to Kr-like are used to investigate the λ_{3l} parameters with a fixed inner core determined from the previous set of sequences. The optimised λ_{3l} values are shown in figure 1d−f, and the λ_{4f} in figure 1g. The overall deviation of the values from unity is lower than that found for λ_{2l} and λ_{1s} and display a slower decay to unity as Z_0 increases. The overlap of the λ_{3l} values occurs for Br-like and Kr-like and therefore these values are fixed as the inner core (in addtion to those from Mg-like) for the sequences from Rb-like onwards. For Rb-like to Kr-like, the optimised λ_{4l} values all have approximately the same values as those shown in remain 1g for Br-like and Kr-like.

The strategy outlined aboved is firstly carried out with $\lambda_{nl} = 1$ as the starting

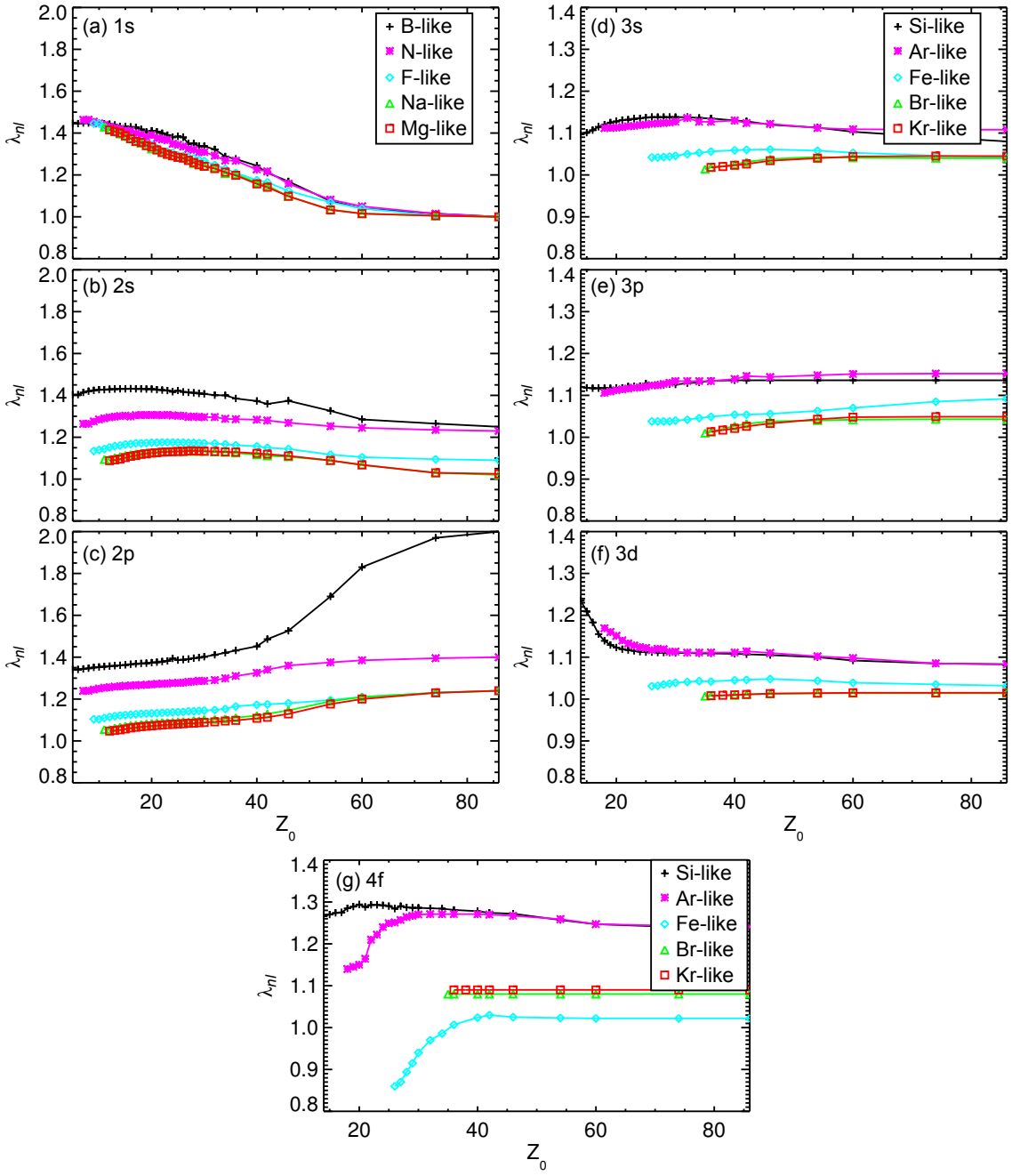

Figure 1. Optimised radial scaling parameters as a function of element charge for different iso-electronic sequences. In (a−c), the 1s, 2s, and 2p orbital scaling parameters are shown for sequences: B, N, F, Na, and Mg -like. The $n = 3$ and 4f orbital scaling parameters are shown in (d−f) and (g), respectively for sequences: Si, Ar, Fe, Br, and Kr -like. The inner orbital scaling parameters in d−g are set to those values shown for the Mg-like sequence in a−c.

conditions in the minimisation. Once a full set of optimised parameters have been determined for every ion, a second iteration of the optimisation is then performed. This time, the starting λ_{nl} values are set to those obtained from the first iteration. A spline fit of the scaling parameters along an iso-electronic sequence is used to identify and

correct any anomolous parameters obtained from the initial minimisation.

3. Atomic structure accuracy

Spectral line emission driven by electron excitation is dependent on the radiative rates (A-values), energy levels, and electron impact collision strengths. In this study, the accuracy of the oscillator strengths, $f_{j\rightarrow i} \propto A_{j\rightarrow i} g_i/g_j$, where g_i is the statistical weight of level i, and energy levels E_i are examined. The electric dipole matrix elements, and hence f values, are equivalent in the length or velocity gauge as

$$f_k = \frac{2m\Delta E_k}{\hbar^2} |\langle i|\mathbf{x}|j\rangle|^2 = \frac{i2m}{\hbar^2} |\langle i|\mathbf{v}|j\rangle|^2 \tag{1}$$

where subscript k corresponds to transition $j \rightarrow i$. However, in multi-electron atoms, the approximate wavefunctions used can give rise to differences between the oscillator strength calculated in length or velocity gauges. Gauge invariance of the radiation matrix elements is a necessary, but not sufficient, condition to ensure the absolute physical accuracy of radiative transition rates and the atomic structure in general [23]. A further check of the atomic structure accuracy involves comparison of the energy levels with values quoted from the NIST database (which provides a combination of experimental and calculated energy levels) and from those calculated using the Hartree-Fock relativistic code by Cowan [9].

Since this study is not focused on any particular emission lines, but rather on all transitions contributing to the total radiated power of an ion, the uncertainties are quantified using an average metric over each ion, weighted by the strongest dipole transitions. AS outputs the weighted length and velocity oscillator strengths $gf^{(len),(vel)}$, therefore the deviation between the two gauges is firstly defined as

$$\delta_k = \frac{|gf_k^{(\mathrm{len})} - gf_k^{(\mathrm{vel})}|}{\max(gf_k^{(\mathrm{len})}, gf_k^{(\mathrm{vel})})} \tag{2}$$

A weighting factor w_k is introduced, $\overline{\delta_z} = \sum_k w_k\delta_k / \sum_k w_k$, to provide a single weighted value for each ion z. This weighting factor is defined as

$$w_k = \frac{A_k^{(\mathrm{opt})} - A_k^{(\mathrm{def})}}{2} \tag{3}$$

where (opt) and (def) correspond to the optimised and default AS calculations.

Lastly, the combined energy level and radiative data accuracy can be quantified for an ion by using a collisional-radiative model to calculate and compare radiated line power coefficients,

$$\mathcal{PLT} = \sum_{i,j} \Delta E_{j,i} A_{j\rightarrow i} \mathcal{F}_{j,1}^{exc} \tag{4}$$

where $\mathcal{F}_{j,1}^{exc}$ is the component of the population of the jth level associated with the ground level normalised by the electron density. In this study, Cowan's code is used to

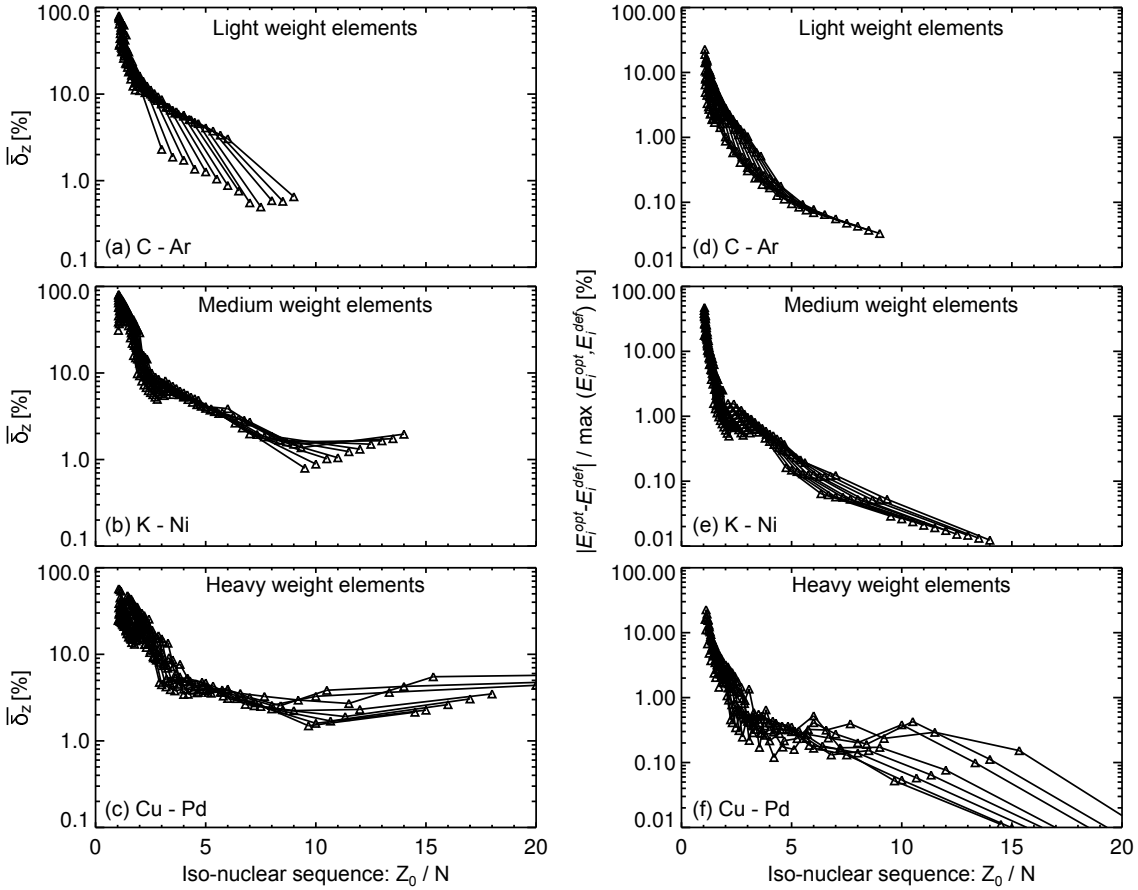

Figure 2. Figures a-c show the A-value weighted difference of the length and velocity gauges, summed over all electric dipole transitions determined from a default AS calculation, is shown for each ion (excluding H-like and neutrals) of an iso-nuclear sequence. Figures d-f show the average energy level difference from a default and optimised AS calculation for the equivalent set of ions. Light weight elements from C-Ar are shown in the top panels, medium weight elements from K-Ni in the middle panels, and heavy weight elements from Cu-Pd in the lower panels. The x-axis has been normalised to Z_0/N, where Z_0 is the nuclear charge and N is the number of electrons.

calculate the $\mathcal{PLT}$ for comparison with AS. The plane-wave Born approximation is used in both codes to calculate the electron impact collision strengths for each transition.

3.1. Oscillator strengths

Using $\overline{\delta_z}$, it is possible to first assess the validity of the default AS calculations grossly across a range of ions. Figures 2a-c compare the default $\overline{\delta_z}$ as a function Z_0/N where N is the number of electrons for all ions (excluding hydrogenic) in the range of (a) C−Ar, (b) K−Ni, and (c) Cu−Pd. The sensitivity to optimisation is typically negligible when $\overline{\delta_z} \leq 10\%$. This decrease in $\overline{\delta_z}$ typically occurs at a critical Z_0/N value, denoted x^{crit}, of $x^{crit} \approx 1.5$ for light-weight ions, $x^{crit} \approx 2.0$ for medium-weight ions, and $x^{crit} \approx 2.5$ for heavy-weight ions.

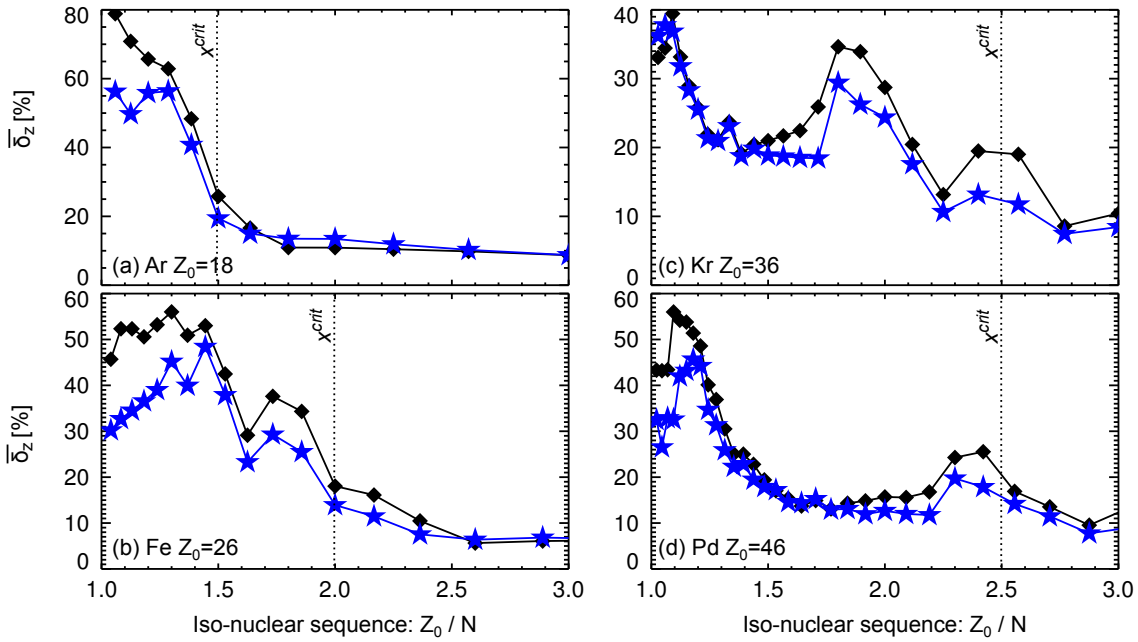

Figure 3. The A-value weighted difference of the length and velocity gauges, summed over all electric dipole transitions determined from a default (black diamonds) and optimised (blue stars) AS calculation, is shown for ions of the (a) Ar, (b) Fe, (c) Kr, and (d) Pd iso-nuclear sequence. The x-axis has been normalised to Z_0/N, where Z_0 is the nuclear charge and N is the number of electrons.

The default and optimised $\overline{\delta_z}$ parameters are shown together as a function of Z_0/N in figure 3 for four iso-nuclear sequences: Ar, Fe, Kr, and Pd. Overall, the most significant reduction in $\overline{\delta_z}$ occurs either for ions in the range of $Z_0/N \leq x^{crit}$ or for ions with an open d shell. The sequences with an open p shell show little difference with the optimised λ_{nl} values.

3.2. Energy levels

The percentage energy level differences between the optimised and default AS calculations are shown in figures 2d-f. The energy levels change by $\leq 1\%$ for $Z_0/N > x^{crit}$; however differences of up to $\approx 50\%$ are found for ions $Z_0/N \leq x^{crit}$. Differences of $\leq 1\%$ are insignificant for calculations of radiated line power coefficients; however spectral line identification and fitting typically require an accuracy of $\leq 0.1\%$. Note that these differences do not quantify the error between code and experiment; they only show the change induced by optimisation.

A qualitative comparison of the energy levels from the AS default and optimised calculations, the NIST database, and Cowan's code are shown for Ar^{+}, Ar^{2+}, and Ar^{3+} in figures 4a−c and for Fe^{+}, Fe^{2+}, and Fe^{3+} in figures 4d−f, respectively. The levels are grouped by colour into their respective configuration. The energy level count for a configuration is complete for both AS and Cowan calculations, however the NIST energy levels are not always necessarily complete. Furthermore, only levels from the AS

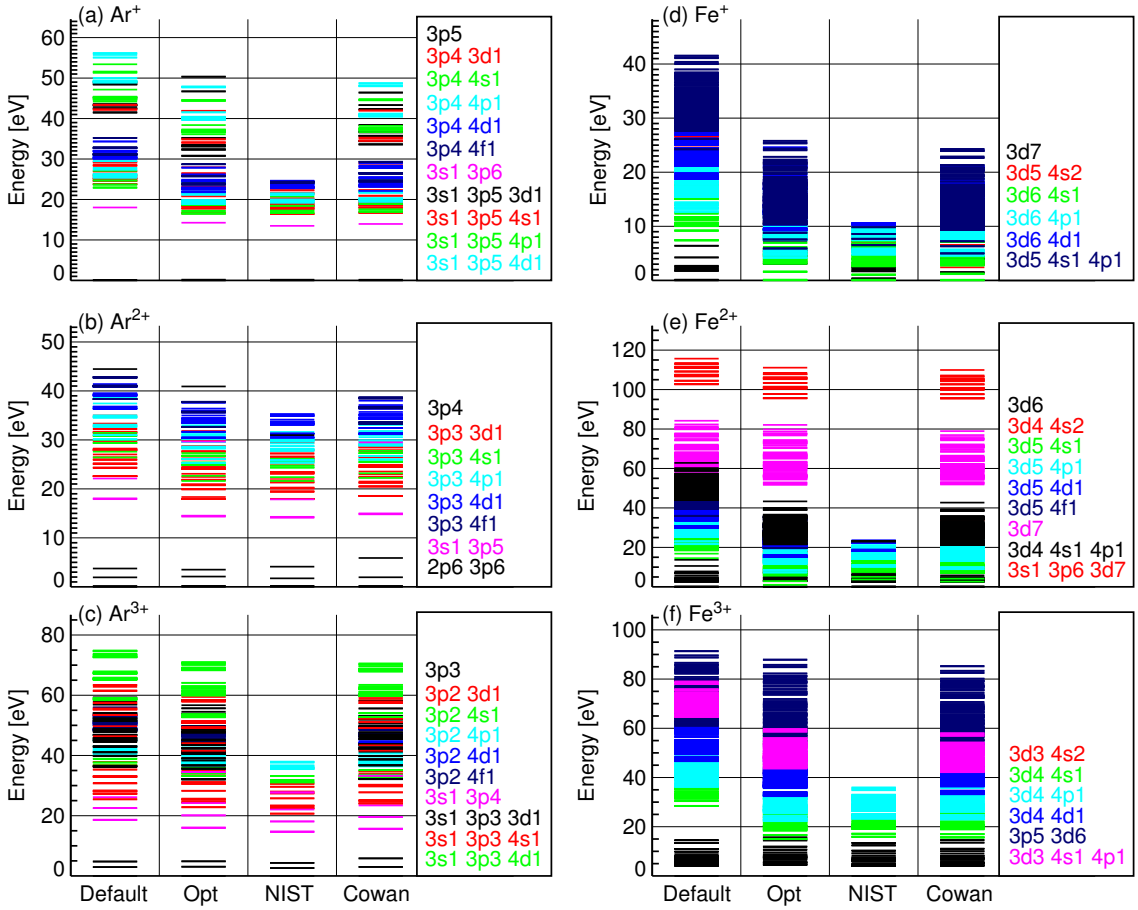

Figure 4. Energy levels from the AS default and optimised calculations, the NIST database, and the Cowan code are shown in four columns for Ar^{+}, Ar^{2+}, and Ar^{3+} in a−c and for Fe^{+}, Fe^{2+}, and Fe^{3+} in d−f, respectively. The levels are grouped by colour into their respective configuration.

calculation with parent configurations that are present in either the Cowan calculation or the NIST database are shown. The optimised centroid energy of each configuration shifts significantly to values in much closer agreement to NIST (where available) and those calculated using Cowans code. Manual adjustment of the scaling parameters could provide better agreement for specific energy levels, for example the high energy levels of the Fe^{3+} 3p5 3d6 configuration; however, for investigations of radiated line power coefficients, the improvement from the optimisation is sufficient (as shown next).

3.3. Radiated line power coefficients

Calculations of the $\mathcal{PLT}$s are carried out firstly in level (ic) resolution. For each ion, the radiation missed due to truncation of the configuration sets (to within computer limits) is estimated by multiplying the ic-resolved $\mathcal{PLT}$s by the ratio of configuration averaged (ca) $\mathcal{PLT}$s with large (denoted cl) and truncated (denoted cs) configuration sets, as described in [12]. Four different calculations are discussed below: Cowan with PWB; optimised AS with PWB and with DW; and default AS with PWB. Since Cowan is

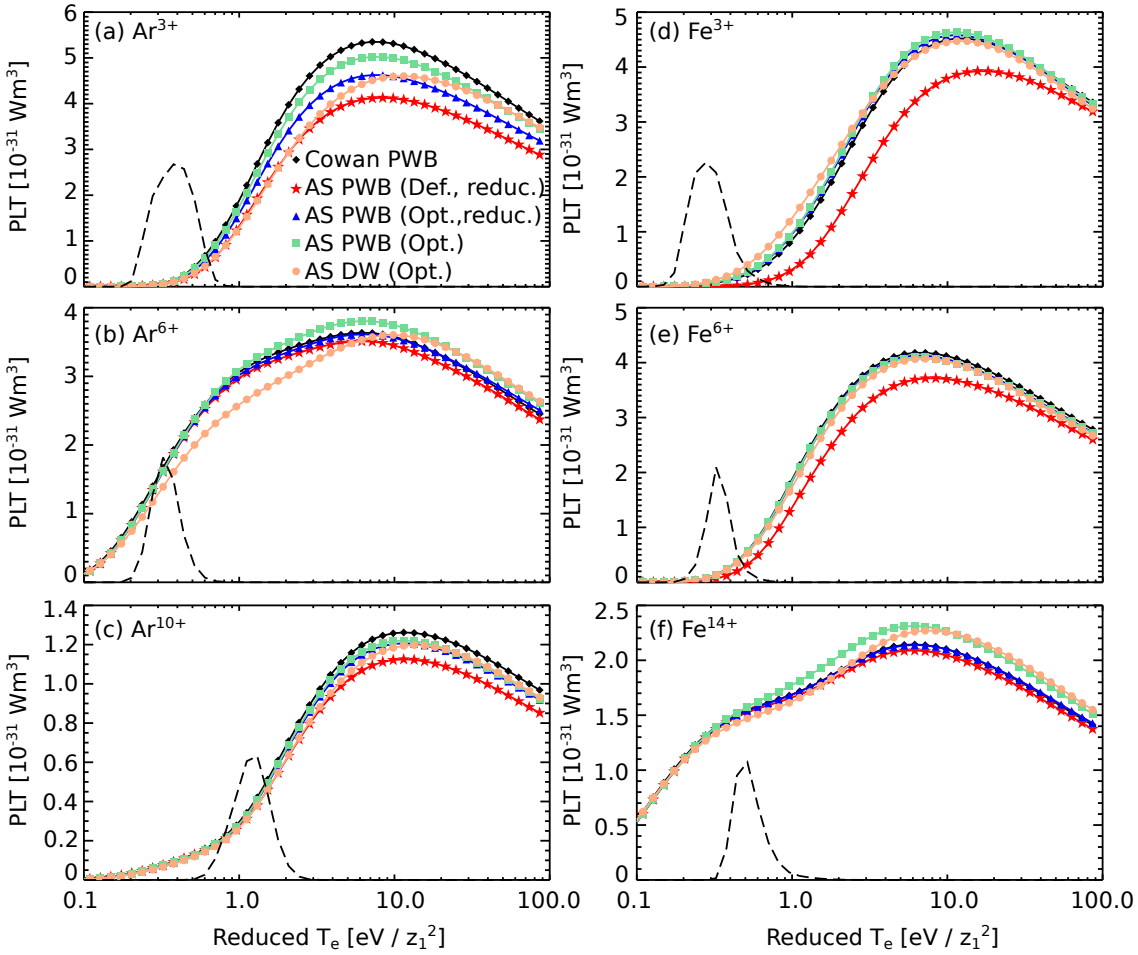

Figure 5. Comparisons of radiated line power coefficients as a function of the reduced temperature for various ions: (a) Ar^{3+}, (b) Ar^{6+}, (c) Ar^{10+}, (d) Fe^{3+}, (e) Fe^{6+}, and Fe^{14+}. The *ic* calculation for both codes uses the same truncated configuration set and top-up correction as described in [12]. The normalised fractional abundances of each ion are shown by the dashed lines.

restricted to transitions up to magnetic dipole, whereas AS includes all possible radiative data, two further AS calculations with a reduced set of PWB transitions are compared.

$\mathcal{PLT}$s for three Ar ions (Z=3,6,10) and three Fe ions(Z=3,6,14) are shown in figure 5. For all ions, the optimised AS $\mathcal{PLT}$s with PWB (blue triangles) show better agreement with the Cowan $\mathcal{PLT}$s (black diamonds) in comparison to the default values (red stars). Differences of up to $\approx 30\%$ between the default and Cowan $\mathcal{PLT}$s (red stars vs. black diamonds) are found for the ions within $Z_0/N < x^{crit}$; however the agreement improves as the ion charge increases. The difference between the blue triangles and green squares indicates improvements of up to $\approx 10\%$ gained by including the full set of transition data. A similar improvement is gained by using collision strengths calculated using DW instead of PWB. Although the overall accuracy of each $\mathcal{PLT}$ is not necessarily an accumulation of each source of uncertainty, it is clear that an accurate atomic structure is necessary to avoid uncertainties larger than $\approx 10\%$.

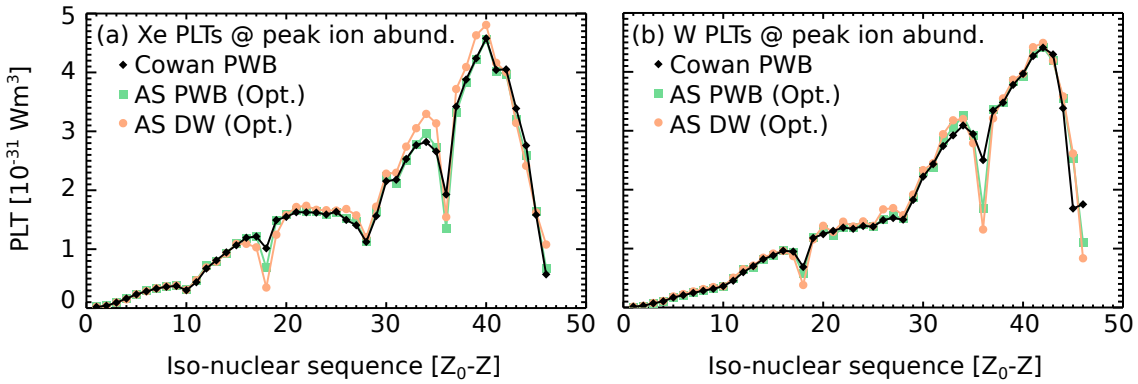

Figure 6. Comparisons of radiated line power coefficients interpolated at the temperature of peak ion abundance for every ion of (a) Xe and (b) W up to Pd-like.

For the ions of heavier elements, such as Xe and W, the optimisation is required most significantly for ions with $Z_0/N < 2.5$, corresponding to Ti-like Xe^{32+} and Zn-like W^{44+}. Optimised AS and Cowan $\mathcal{PLT}$s, interpolated at the temperature of peak ion abundance, are shown in figure 6 for each ion of Xe and W (up to Pd-like). The agreement between the optimised AS and Cowan PWB $\mathcal{PLT}$s is within $\approx 10\%$. DW calculations differ from PWB by up to $\approx 15\%$ at the temperature of peak ion abundance.

Larger discrepancies between the optimised AS and Cowan PWB $\mathcal{PLT}$s are found for the Pd-like, Kr-like, and Ar-like ions. In [12], the set of Cowan PWB collision strengths for these specific ions were supplemented with DW collision strengths from a default AS calculation. These ions were also of particular interest due to the significant differences between the *ic* and *ca* resolved $\mathcal{PLT}$s. The approximation made in [24] is that $\mathcal{PLT}$s for W are adequately described by *ca*-resolved PWB calculations using Cowan. However, a substantial decrease in the $\mathcal{PLT}$s in only the *ic*-resolved calculations were found for the Pd-like, Kr-like, and Ar-like ions of W. This is due to high J, *ic*-resolved metastables found in the first excited (opposite parity) configuration which is strongly dipole in the *ca*-resolved calculation. However, these anomalies were previously explained to be caused by missing physics from the Cowan PWB calculation [24].

Since this potential drop in radiation for Pd-like W^{28+} occurs at approximately $T_e = 800 - 1000$ eV, where the radiation could be influencing the behaviour of the edge plasma in JET [25], the W^{28+} $\mathcal{PLT}$s are re-assessed using optimised DW collision strengths and including all possible transitions. The results are shown in figure 7. The *ca*-resolved (*cs* and *cl*) $\mathcal{PLT}$s are approximately an order of magnitude greater than the *ic*-resolved $\mathcal{PLT}$s from both AS and Cowan. Optimised DW $\mathcal{PLT}$s do not differ sufficiently from Cowan in the region of peak ion abundance suggesting that spin-change and higher order multipole transitions do not de-populate the metastable levels. It is noted that ion-impact collisions are missing and that R-matrix collision strengths would offer a further refinement to the $\mathcal{PLT}$s; however these are not expected to significantly change the population of the metastable levels in these particular ions.

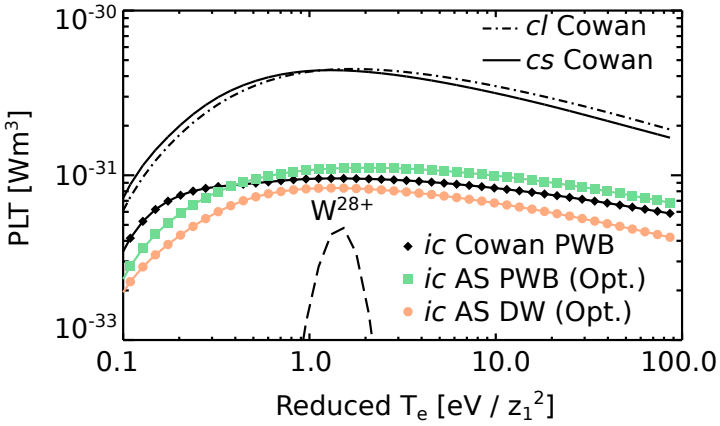

Figure 7. Comparisons of radiated line power coefficients as a function of the reduced temperature for Pd-like W^{28+}. *ic* resolved coefficients are shown by the filled symbols for Cowan and AS, while *ca* resolved coefficients are shown by the dashed and solid lines. *cl* and *cs* correspond to *ca* calculations with large and truncated configuration sets, respectively.

4. Data archiving

The AS calculations are carried out within the ADAS framework and the data is made available via OPEN-ADAS at `http://open.adas.ac.uk`. Source and output data are stored in ADAS data format (*adf*) files for which the formal format specification is documented on the ADAS website [8]. The optimised fundamental atomic structure data and DW effective collision strengths are archived in *adf04* files, which are separate files for each ionisation stage in *ic* resolution. The derived $\mathcal{PLT}$ coefficients are archived in iso-nuclear sets with one file per element in the *adf11* format. Note that data from [12] are used to complete the iso-nuclear sets for ions between Pd-like and W-like and to provide the power truncation top-up estimate. AS orbital scaling parameters are archived in a unique *adf54* file.

In ADAS nomenclature, the files will be labelled with the 'year' 42 identifier and author initials: the pattern for *adf04* and *adf11* will be ssh42_<res>#<sym>< Z_1 >.dat and plt42_<sym>.dat, respectively, where <res> is *ic*, <sym> is ar, fe, kr, xe, or w, and $< Z_1 >$ is the ion charge from 0 to $Z_0 - 1$.

5. Conclusions

The inaccuracy of the energy levels and spontaneous decay rates calculated using the Thomas-Fermi-Dirac-Amaldi model potential with radial orbital scaling parameters set to unity in the Autostructure code give rise to uncertainties of up to $\approx 30\%$ in the radiated line power coefficients. This is demonstrated by comparisons of impurity line power coefficients calculated with Cowan's code in the plane-wave Born approximation over a range of medium and heavy weight impurities.

A systematic approach to producing a table of optimised scaling parameters for

every orbital of any ion up to and including the Pd-like iso-electronic sequence is presented. Calculations using the optimised scaling parameters typically improve the agreement of the line power coefficients from Autostructure and Cowan to $\leq$ 5%. Furthermore, it is shown that the energy levels change by up to $\approx$ 50% and typically match better with energy levels from NIST and Cowan's code. Gauge invariance theory is used to demonstrate that the accuracy of the oscillator strengths, averaged over the dipole allowed transitions, are improved for each ion.

These scaling parameters may not be compatible with non-relativistic calculations, which are a neccessary requirement for R-matrix calculations, and will likely require further optimisation for detailed studies of individual, non-dipole line strengths. The configuration sets associated with each iso-electronic sequence were chosen to account for configuration interaction and to minimise the error arising from the truncation of configurations required for level-resolved calculations. These scaling parameters are therefore recommended as an improved set of default conditions to use in the Autostructure code for relativistic calculations coupled with plane-wave Born or distorted wave collision strength calculations of radiated line power coefficients.

The improvement in accuracy of the atomic structure coefficients from Autostructure now allows for baseline calculations of the line power coefficients in the distorted-wave approximation. The new line power coefficients differ from previous baseline coefficients in the plane-wave Born approximation by up to 15%. Further work is in progress to characterise the remaining uncertainty of the composite cooling function due to the fractional ion abundance inaccuracy.

Acknowledgements

S. Henderson gratefully acknowledges Prof. N. Badnell for his helpful advice in running the Autostructure code. This work was funded in part by the RCUK Energy Programme [under grant EP/P012450/1] and by ADAS and its consortium members.

References

[1] J. M. M. Burgos, S. D. Loch, C. P. Ballance, and R. F. Boivin, Astron. Astrophys. **500**, 1253 (2009).
[2] P. J. Storey and T. Sochi, Mon. Not. R. Astr. Soc. **456**, 1974 (2016).
[3] S. S. Henderson *et al.*, Nucl. Fusion **58**, 016047 (2018).
[4] M. Kovari *et al.*, Fusion Eng. Design. **89**, 3054 (2014).
[5] M. Kovari *et al.*, Fusion Eng. Design. **104**, 9 (2016).
[6] C. Reux *et al.*, Nucl. Fusion **55**, 073011 (2015).
[7] H. Lux, R. Kemp, D. J. Ward, and M. Sertoli, Fusion Eng. Design. **101**, 42 (2015).
[8] H. P. Summers, The ADAS manual, version 2.3, http://www.adas.ac.uk, 2001.
[9] R. D. Cowan, The Theory of Atomic Structure and Spectra (University of California Press, Berkeley, 1981).
[10] N. R. Badnell, J. Phys. B: At. Mol. Phys. **19**, 3827 (1986).
[11] N. R. Badnell, Comput. Phys. Commun. **182**, 1528 (2011).
[12] S. S. Henderson *et al.*, Plasma Phys. Control. Fusion **59**, 055010 (2017).

[13] W. Eissner and H. Nussbaumer, J. Phys. B: At. Mol. Phys. **2**, 1028 (1969).
[14] M. A. Bautista *et al.*, Astron. Astrophys. **508**, 1527 (2009).
[15] P. J. Storey, T. Sochi, and N. R. Badnell, Mon. Not. R. Astr. Soc. **441**, 3028 (2013).
[16] P. J. Storey and T. Sochi, Mon. Not. R. Astr. Soc. **459**, 2558 (2016).
[17] M. Witthoeft, A. Whiteford, and N. Badnell, J. Phys. B: At. Mol. Opt. Phys. **40**, 2969 (2007).
[18] G. Liang and N. Badnell, Astron. Astrophys. **518**, A64 (2010).
[19] G. Liang, N. Badnell, and G. Zhao, Astron. Astrophys. **547**, A87 (2012).
[20] L. Menchero, G. Del-Zanna, and N. Badnell, Astron. Astrophys. **566**, A104 (2014).
[21] L. Menchero, G. Del-Zanna, and N. Badnell, Astron. Astrophys. **572**, A115 (2014).
[22] D. Kasen, N. R. Badnell, and J. Barnes, Astrophys. J. **774**, 13 (2013).
[23] I. P. Grant, J. Phys. B: At. Mol. Phys. **7**, 1458 (1974).
[24] T. Pütterich *et al.*, Plasma Phys. Control. Fusion **50**, 085016 (2008).
[25] E. R. Solano *et al.*, in Characterising W radiation in JET-ILW plasmas, edited by P. Mantica, G. Giruzzi, M. Fajardo, and T. Gans (European Physical Society, ADDRESS, 2016), Vol. P2.005.